Ionization of lithium by impact of fast bare ions

M. R. Fiori,[1] Ginette Jalbert,[1] C. E. Bielschowsky,[2] and W. Cravero[3]
[1]*Instituto de Física, Universidade Federal do Rio de Janeiro, Caixa Postal 68528, Rio de Janeiro, 21945-970, RJ, Brazil*
[2]*Instituto de Química, Departamento de Físico-Química, Universidade Federal do Rio de Janeiro, Rio de Janeiro, 21949-900, RJ, Brazil*
[3]*Departamento de Fisica, Universidad Nacional del Sur, Avenida Pellegrini 250, 8000 Bahía Blanca, Buenos Aires, Argentina*
(Received 7 December 2000; published 5 June 2001)

Double differential and total cross sections (DDCS and TCS) for ionization of Li by fast bare ions, namely, H^+, He^{2+}, N^{7+}, and Ar^{18+}, are calculated within the continuum distorted wave eikonal-initial-state aproximation employing several static atomic potentials. Both the DDCS and the TCS cross sections, calculated using optimized potential method and $X_\alpha(\alpha=0.781)$ potentials, are nearly equivalent, but one pseudopotential tested, already successfully used in other branches of physics and chemistry, led to the wrong angular dependence and could present serious problems for fast ion-atom collision study.

DOI: 10.1103/PhysRevA.64.012705 PACS number(s): 34.50.Fa

I. INTRODUCTION

The informations obtained from collisions of electrons, protons, and multiply charged ions with lithium atoms are very useful for spectroscopical diagnostics of magnetically confined plasmas [1]. Otherwise, cross-section measurements and calculations for these collisions are very interesting by themselves. The fact that lithium has two tightly bound $1s$ electrons (59 eV) and one weakly bound $2s$ electron (5.5 eV) favors the test of different target wave functions with the same collisional model.

One particular case, the ionization of lithium by bare ions, has been studied by Shah *et al.* [2] and Dubois [3], who measured the total lithium ionization cross section for energies in the interval 15 keV/u–2.1MeV/u using protons and helium ions as projectiles. Also angular and energy distributions of ejected electrons from lithium by 10.6 MeV/u N^{7+} ion impact were measured by Skogvall *et al.* [4]. Cross sections for single ionization of lithium by 95-MeV Ar^{18+} impact ion, looking especially for two-and three-body effects in analogy with photoionization, were measured by Stolterfoht *et al.* [5] that proposed a decomposition of the total cross section in terms of multipoles. Wütte *et al.* [6] have collected, in 1997, the available experimental and theoretical total cross section data for collision of Li atoms, in the ground and excited (up to $n=3$) states, with electrons, protons, and multiply charged ions.

The first Born approximation (FBA) was used in the early sixties to calculate total cross sections (see Ref. [7]), presenting a reasonable agreement with the experiments for small values of the Bohr parameter Z_p/v_p, where Z_p is the projectile charge and v_p its initial velocity. In particular, ionization of lithium atoms by proton impact was first considered by McDowell and Peach [8] and further calculations were done by Peach [9]. It is now well known that calculations of the differential cross sections within FBA, even at the small value of Z_p/v_p, miss out some important features, as they do not take into account the post-collisional interaction between the ejected electron and the projectile. One approximation including this interaction is the continuum distorted wave eikonal-initial-state (CDW-EIS), originally developed by Crothers and McCann [10], and first used for Li targets by McCartney and Crothers [11] in 1993. In the latter, double-differential cross sections (DDCS) for $1s$ and $2s$ ionizations of Li by protons and He^{2+} were calculated, with the target being described by a Roothan-Hartree-Fock wave function [12] for the initial bound state and an effective charge continuum wave function for the ejected electron; interesting features arose related to two-center effects not described by the previous FBA work. The work of Sánchez *et al.* [13] extended this analysis, within the same theoretical approach and process, to the triply differential cross section.

Skogvall *et al.* [4] analyzed their experimental results of ionization of Li atoms by N^{7+} ions using the CDW-EIS approximation with *Hartree-Fock-Slater* (HFS) $X\alpha$ [14] wave functions as tabulated by Herman and Skilman [15]. They calculated the differential cross sections, estimating the importance of different multipole terms in the collision process, and compared them with the experimental results. In their work, hydrogenic wave functions were also used and the influence of the target description on the ionization cross section was discussed, and marked differences with the description of the target appeared. The influence of the description of the target in the total cross sections was also emphasized in the work of Kirchner *et al.* [16]. They used different single-particle potentials within the CDW-EIS method to determine the total cross sections for single ionization of Ne and Ar atoms by protons and the basis generator method [17], a coupled-channel approach in terms of structurally adapted basis functions, to determine the net electron loss.

Finally, within the framework of the Born approximation, Stolterfoht *et al.* [5] measured the cross section for single ionization of Li by 95-MeV Ar^{18+}, separating the contribution of the *2s* orbital, which has a node, into two parts: the outer part of this orbital being responsible for the peak close to 90° and the inner part together with the $1s$ orbital, responsible for the broad Compton profile.

In the present paper, we study the dependence of the double differential cross sections (DDCS), as well as the total cross section (TCS), for ionization of Li atoms by H^+, He^{2+}, N^{7+}, and Ar^{18+} ions, upon the choice of the target description, that is, the single-particle potential used in the

 ©2001 The American Physical Society

determination of the bound initial and continuum final electronic wave function of the target electron. The dynamics of the collision is described by CDW-EIS [10]. We use four different types of model wave functions, the ground and ionized states being obtained from (1) the pseudopotential of Bachelet *et al.* [18], (2) the single-particle potential calcultated with the *optimized potential method* (OPM) [19], and (3) the Hartree-Fock-Slater $X\alpha$ [14] wave functions. Also, as the Z_{eff} approximation has been extensively used, we consider instructive for comparison reasons to include some results calculated within this model. In the latter case, the ground state was obtained by the Roothan-Hartree-Fock wave function [12] and the ionized states described by an effective charge $Z_{\text{eff}}=\sqrt{-2n^2\varepsilon_n}$ continuum (Coulomb) wave function, where ε_n corresponds to the ionization potential of the n shell.

The different bound and continuum wave functions obtained from the single-particle potentials are compared one with the others. The DDCS, as well as the TCS, are also compared with the available experimental and theoretical results. In particular, we look for the influence of the potential upon the angular momentum decomposition of the cross section. Emphasis is placed in presenting theoretical results that can be compared with available experimental and other theoretical calculations.

II. THEORY

A. Continuum distorted wave

We calculate the cross sections for single ionization of lithium by bare ions impact (H^+, He^{2+}, Ni^{7+} and Ar^{18+}) within the CDW-EIS model introduced by Crothers and McCann [10]. The goal of this approximation is to treat nonperturbatively the initial (final) Coulomb interaction between the projectile and the active electron while taking part of the kinetic energy as perturbation. CDW-EIS incorporates an eikonal phase distortion on the initial state and a final continuum wave function centered on both the target and projectile nuclei and by this way, the ejected electron moves in the continuum of both the residual target and the projectile. The two-center effects, which are accounted for in this model, are important in general for the analysis of the differential cross sections and in particular, for the analysis of the total cross sections at intermediate energies.

The fivefold differential cross section is written as

$$\frac{d^5\sigma}{dE_e d\Omega_e d\Omega_P}=\frac{\mu^2}{(2\pi)^2}|T_{if}|^2, \tag{2.1}$$

where μ is the reduced mass of the projectile-target system and T_{if} is the transition matrix element. The other differential and total cross sections are obtained by integration of Eq. (2.1). After removing the internuclear potential, the transition matrix in the post form is given by

$$T_{if}=\langle\chi_f^-|W_f^\dagger|\chi_i^+\rangle, \tag{2.2}$$

with the initial eikonal distorted wave function being

$$\chi_i^+=\phi_i(\mathbf{x})L_i^+(\mathbf{s})\exp(i\mathbf{K}_i\cdot\mathbf{R}) \quad \text{with}$$

$$L_i^+(\mathbf{s})=\exp\left(-i\frac{Z_P}{v}\ln(vs+\mathbf{v}\cdot\mathbf{s})\right) \quad \text{and}$$

$$\phi_i(\mathbf{x})=\frac{u_{n_i l_i}}{x}Y_{l_i}^{m_i}(\hat{\mathbf{r}}),$$

$\mathbf{s}$, $\mathbf{R}$, $\mathbf{x}$, being, respectively, the electron-projectile, projectile-nucleus, and atomic coordinates, and $\mathbf{K}_i$ is the initial momentum of the projectile in the center-of-mass system.

The final Coulomb distorted wave is given by

$$\chi_f^-=\phi_f^-(\mathbf{x})D_f^-(\mathbf{s})\exp(i\mathbf{K}_f\cdot\mathbf{R}) \quad \text{with}$$

$$D_f^-(\mathbf{s})=\exp\left(\frac{\pi}{2}\xi\right)\Gamma(1-i\xi)_1F_1 \times[-i\xi,1,-i(ps+\mathbf{p}\cdot\mathbf{s})] \quad \text{and}$$

$$\phi_f^-(\mathbf{x})=\frac{1}{x\sqrt{k}}\sum_{lm} i^l\exp(-i\delta_l)u_{lk}(x)[Y_l^m(\hat{\mathbf{r}})]^*Y_l^m(\hat{\mathbf{k}}),$$

$\mathbf{k}$ being the momentum of the ejected electron in the target frame, $\mathbf{p}=\mathbf{k}-\mathbf{v}$ the momentum of the electron in the projectile frame, and $\xi=Z_P/p$. The continuum eigenstate $\phi_f^-(\mathbf{x})$ is normalized on the energy scale (with $\varepsilon_f=k^2/2$) through the condition

$$u_{lk}(x)\to\sqrt{\frac{2}{\pi k}}\sin\left(kr+\frac{1}{k}\ln(2kr)-\frac{l\pi}{2}+\delta_l\right)$$

and δ_l is the total phase shift.

The action of the perturbation on the final state is given by

$$W_f\chi_f^-=[-i\mathbf{k}\phi_f^-(\mathbf{x})+\nabla_{\mathbf{x}}\phi_f^-(\mathbf{x})]\cdot\nabla_{\mathbf{s}}D_f^-(\mathbf{s}). \tag{2.3}$$

The transition matrix T_{if} can then be written as

$$T_{if}=\mathbf{A}(\mathbf{q})\cdot\mathbf{B}(\mathbf{q}), \tag{2.4}$$

where $\mathbf{A}(\mathbf{q})$, given by formula (20) of Ref. [11], depends on the velocity and charge of the projectile and on the electron momentum, being independent of the atomic wave function. The term in Eq. (2.3) that involves the gradient is calculated with the help of [20]

$$\nabla[f(r)Y_l^m(\hat{\mathbf{r}})]=-\sqrt{\frac{l+1}{2l+1}}\left(\frac{df}{dr}-\frac{l}{r}f\right)\mathbf{Y}_{lm}^{l+1}(\hat{\mathbf{r}}) +\sqrt{\frac{l}{2l+1}}\left(\frac{df}{dr}+\frac{l+1}{r}f\right)\mathbf{Y}_{lm}^{l-1}(\hat{\mathbf{r}})$$

and, in the case of a initial state of s symmetry (lithium), we use

$$\int \exp(i\mathbf{q}\cdot\mathbf{r})\mathbf{Y}_{LM}^{J}(\hat{\mathbf{r}})d\Omega = 4\pi i^{L} j_{L}(qr)\mathbf{Y}_{LM}^{J}(\hat{\mathbf{q}}).$$

Then, the $\mathbf{B}(\mathbf{q})$ factor of Eq. (2.4) reads

$$\mathbf{B}(\mathbf{q}) = -i\sum_{lm}\left[\mathbf{k}R_{0_{lk}}(q)Y_{l}^{m}(\hat{\mathbf{q}}) + R_{1_{lk}}(q)\mathbf{Y}_{lm}^{l+1}(\hat{\mathbf{q}}) + R_{2_{lk}}(q)\mathbf{Y}_{lm}^{l-1}(\hat{\mathbf{q}})\right]\left[Y_{l}^{m}(\hat{\mathbf{k}})\right]^{*}\exp(i\delta_{l}) \quad (2.5)$$

with

$$R_{0_{lk}}(q) = 4\pi\int u_{lk}(x)j_{l}(qx)u_{ns}(x)\,dx, \quad (2.6)$$

$$R_{1_{lk}}(q) = 4\pi\sqrt{\frac{l+1}{2l+1}}\int u_{n_i s}(x)j_{l+1}(qx) \times\left(u'_{lk}(x) - (l+1)\frac{u_{lk}(x)}{x}\right)dx, \quad (2.7)$$

$$R_{2_{lk}}(q) = 4\pi\sqrt{\frac{l}{2l+1}}\int u_{n_i s}(x)j_{l-1}(qx) \times\left(u'_{lk}(x) + l\frac{u_{lk}(x)}{x}\right)dx. \quad (2.8)$$

We note that the first term of $\mathbf{B}(\mathbf{q})$, given in Eq. (2.6), is proportional to the first Born approximation [21], which gives an undistorted initial-state wave function, and a final-state continuum wave function centered only on the target. The sum on m in Eq. (2.5) that represents the product of a vector and scalar spherical harmonics can be expressed in terms of the Legendre polynomials and their derivatives (see formula 7.3.11 of Ref. [20]).

B. Atomic potentials

Ab initio treatment for the continuum atomic wave function is numerically difficult. Nevertheless, very interesting results have been obtained by some authors for the problem of photoionization and electron-impact ionization of atoms and molecules. The work of Burke *et al.* within the matrix R formalism [see Ref. [22]], the work of Venuti *et al.* [23] within a configuration interaction approach, and the one of Machado *et al.* [24] within the multichannel variational Schwinger formalism, are some examples of *ab initio* treatments. In the case of lithium photoionization, Ritchie *et al.* [25] used different local potentials (one was the HFS) and compared the results so obtained with the ones coming from an exact static-exchange calculation, obtaining discrepancies.

The use of precise continuum wave functions for calculating cross sections of ion-atom collisions is numerically very expensive in computation time. For this reason, it becomes necessary to use an approximate effective potential to calculate the continuum atomic wave functions. In this paper, we employ the frozen-core approximation in which the continuum electron moves in the same potential originated by the core in the initial state, leading to a continuum state that is automatically orthogonal to the initial state. These potentials may include some of the correlation effects, but do not include relaxation that may be significant for the ionization of the $1s$ electrons. The ionization potential or binding energy (ϵ) of each orbital was approximated by its corresponding orbital energy.

We have tested different potentials in order to check their influence on the calculated cross sections. The effective potentials should lead to (a) initial bound wave functions reproducing the initial wave function calculated by an *ab initio* calculation, and (b) correct boundary conditions for the continuum wave state, that is, to converge asymptotically to a Coulomb potential with a charge equal to one.

Some of the effective potentials (V_{eff}) available in the literature are

(1) Local-density approximation (LDA) [26]—In ion-atom collision problems, several authors [16,27] use potentials where the nonlocal exchange contribution is approximated by a local function. One of the most commonly used versions of the LDA is the $X\alpha$ approximation, which considers the exchange term proportional to that of an homogenous electron gas where α is an adjustable parameter going from 2/3 to 1. The $X\alpha$ method was originally developed by Slater and it is sometimes called the HFS [14] method. The HFS wave functions of Refs. [16,27] were obtained with $\alpha = 2/3$, and the LDA wave functions of Ref. [16] were calculated with $\alpha = 1$. In the present paper, we use α equal to 0.781 [28], which is considered the best value for Li. A revised version of the Herman-Skillman code was used in order to generate the different Xα potentials [29].

(2) OPM—An efficient approach to find an atomic effective potential is the optimized potential model [19,30,31]. In this procedure an effective local potential, variationally optimized, is obtained. This model provides an effective local potential along with an exchange potential while keeping the degree of accuracy close to the HF level. The numerical effective potential was generated by the code given in Ref. [19].

(3) Pseudopotential of Bachelet *et al.* [18]—The pseudopotentials were introduced to simplify electronic structure calculations by eliminating the need to include atomic core states and the strong potential responsible for binding them [32]. The characteristics of the pseudowave function calculated by the pseudopotential of Bachelet *et al.* [18] are (i) it is nodeless and becomes equal to the true valence wave function beyond some ''core radius'' R_c, (ii) real and pseudovalence eigenvalues agree for a chosen atomic ''prototype'' configuration, (iii) the integrals from 0 to r of the real and pseudocharge densities agree for $r > R_c$ for each valence state (norm conservation); (iv) the logarithmic derivatives of the real and pseudowave function and their first energy derivatives agree for $r > R_c$, and (v) transferability criterion, that is the core portion of the pseudopotential must be transferable to other situations where the external potential has changed, such as in molecules or excited states and where states of interest are at different energies. A complete tabulation of the fitted potentials from H to Pu is given in Ref. [18].

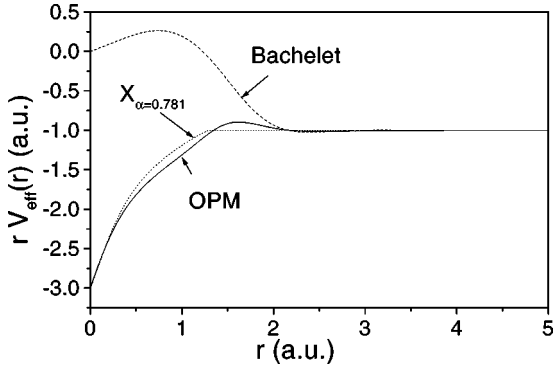

FIG. 1. V_{eff} (a.u.) multiplied by r (a.u.). Solid line, OPM potential; dashed line, Bachelet's pseudopotential; dotted line, X_α ($\alpha=0.781$).

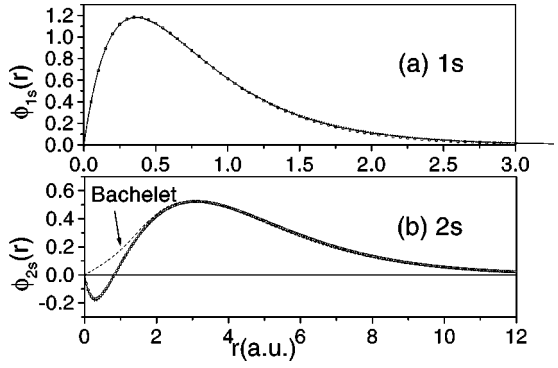

FIG. 2. Bound wave functions, (a) 1s, and (b) 2s. Solid line, OPM potential; dashed line, Bachelet's pseudopotential; dotted line, X_α ($\alpha=0.781$); and short-dotted line, Clementi *et al.* For the wave function 1s, Bachelet's pseudopotential does not exist.

The first three potentials multiplied by r are shown at Fig. 1. Clearly, the OPM results agree with the X_α ($\alpha=0.781$) potential, and both potentials disagree with the Bachelet's potential, especially for small values of r. The repulsive part of the Bachelet's potential represents the action of the electronic core. As expected, the OPM, Bachelet, and X_α ($\alpha=0.781$) potentials reproduce the correct boundary conditions (condition b), that is, converge asymptotically to a Coulomb potential with a charge equal to one.

The influence of these potentials on the discrete 1s and 2s wave functions are shown, respectively, in Figs. 2(a) and 2(b). The wave functions calculated with the X_α ($\alpha=0.781$) and OPM potentials are quite similar, but those calculated with the Bachelet's pseudopotential do not show the correct shape for small values of r. The *ab initio* Clementi *et al.* wave functions [12] are also shown in this figure. We observe that the X_α ($\alpha=0.781$) and OPM wave functions are quite similar to the *ab initio* ones, satisfying the condition (a) which requires that the initial bound wave functions should reproduce the initial wave function calculated *ab initio*.

The effects of the different potentials upon the continuum wave functions may be seen in Figs. 3(a) and 3(b) for the ejected electron energy $\epsilon_e=1$eV ($k=0.27$ a.u.) and $l=0-1$. It is also interesting to look at the internal phase shifts δ_l^{in} defined as the difference between the total phase shifts δ_l and the Coulomb ones δ_l^c. Figures 3(b)–3(d) show δ_l^{in}, respectively, for $l=0-1$ calculated with the different potentials as a function of the electron momentum k. Also in this case, little difference is seen for the phase shifts calculated from the X_α ($\alpha=0.781$) and OPM potentials, but both present remarkable differences when compared to the Bachelet results. The negative phase shifts observed within the Bachelet's potential are a consequence of its internal repulsive part.

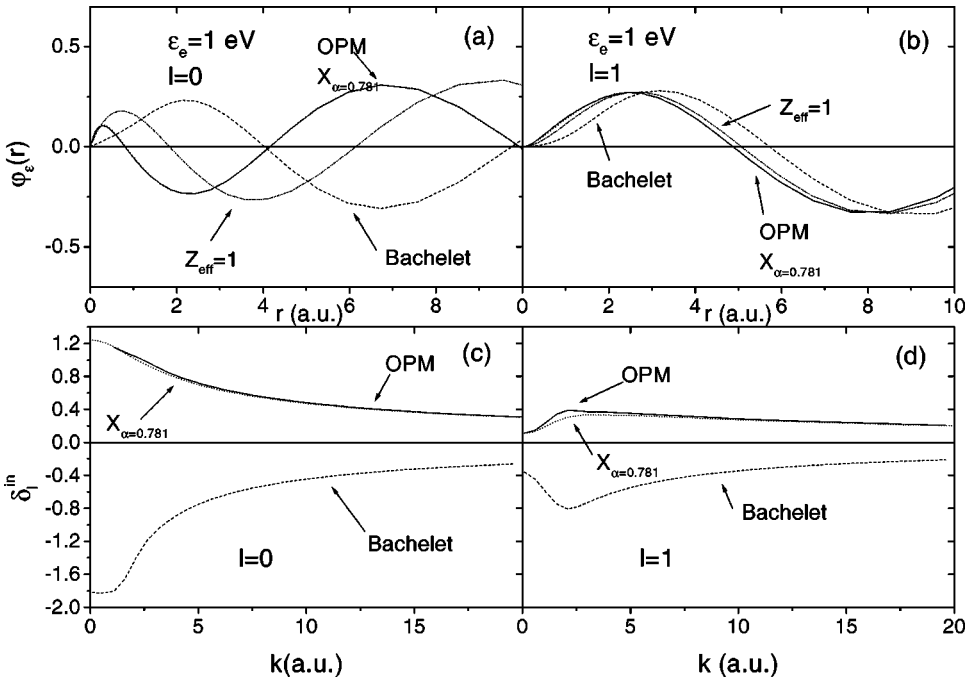

FIG. 3. Continuum wave functions as a function of the radius r (a.u.). Solid line, OPM potential; dashed line, Bachelet's pseudopotential; dotted line, X_α ($\alpha=0.781$); dash-dotted line, $Z_{\text{eff}}=1$. (a) $l=0,\epsilon_e=1$ eV; (b) $l=1,\epsilon_e=1$ eV. Internal phase shifts δ_l^{in} as a function of the electron momentum k. Solid line, OPM potential; dashed line, Bachelet's pseudopotential; the dotted line, $X\alpha$ ($\alpha=0.781$). In (c) $l=0$ and in (d) $l=1$.

C. Numerical procedures

The radial Schrödinger equation was numerically solved, for the above different static potentials, with the code of Ref. [33] in a logaritmic mesh.

For the evaluation of the integrals of Eqs. (2.6), (2.7), and (2.8) we used a cubic spline integration on a given mesh of points. The choice of the grid depends on the largest values of momentum q or k, in such a way that the most oscillated portion of the functions u_{lk} or j_l have more that 40 points per period of oscillation. In all the cases, the values of u_k were approximated, in the chosen grid, by a cubic spline.

For the evaluation of the DDCS we performed the q integration from $(q_{\min} \simeq k_e^2/2 + |\varepsilon_i|/v_p)$ to some value of $q = q_f$ where, in practice, the integral is convergent (for example, in the case of impact of 95-MeV Ar^{18+} for an electron of 10 eV, $q_f = 0.5$ was sufficient). The cross sections were tested with the analytical result for the case of Coulomb potential [11,34,35] and the deviation was less than 1%.

III. RESULTS AND DISCUSSION

A. Results

DDCS and TCS for the ionization of lithium atoms by protons and multicharged ions have been obtained within the CDW-EIS approximation, with the target wave functions calculated with the four potentials described in Sec. II B.

Figure 4 show the DDCS for some selected ejected electron energy (ε_e) as a function of the ejected electron scattering angle (θ_e), for the collision of 10.6-MeV N^{+7} on Li atoms. Together with our results, we show the experimental and theoretical results of Skogvall *et al.* [4] (obtained within the HFS potential $\alpha = 2/3$). The experimental errors were estimated to be up to 30% for the lowest electron energy measurements, less than 20% for energy values between 30 and 100 eV and up to 50% for the measured energies above 100 eV. All the results in this figure correspond to the total ionization of the lithium atoms, i.e., the sum of the contributions of the $1s$ and $2s$ except for the Bachelet's pseudopotential, where no $1s$ wave function type is available, and for Fig. 4(a) (1 eV) where only the $2s$ contribution is theoretically considered.

Figure 5 show our DDCS for the 95-MeV/amu Ar^{18+} and the corresponding contributions to the coherent sum of the monopole, dipole terms and the $l > 1$ terms for the $2s$ electrons emission of 1 eV [Figs. 5(a) and 5(b)] and 10 eV [Figs. 5(c) and 5(d)]. The atomic wave functions were calculated from the OPM and the Bachelet potentials. It is worth mentioning that the OPM and X_α ($\alpha = 0.781$) give the same results.

We also analyze the cross section behavior in the low-energy and small charge cases, considering an H^+ beam of 200 keV, because this energy corresponds to an extreme case where there is a long interaction time between the ejected electron and the projectile.

Angular distributions (DDCS) for 200 keV protons on Li as a function of θ_e for some ejected electron energy are presented in Figs. 6(a)–6(d). Figures 6(a)–6(b) correspond to an ionization of the $1s$ electron for $\epsilon_e = 1$ eV and $\epsilon_e = 100$ eV, respectively, and Figs. 6(c) $\epsilon_e = 1$ eV and 6(d) $\epsilon_e = 100$ eV to an ionization of the $2s$ electron.

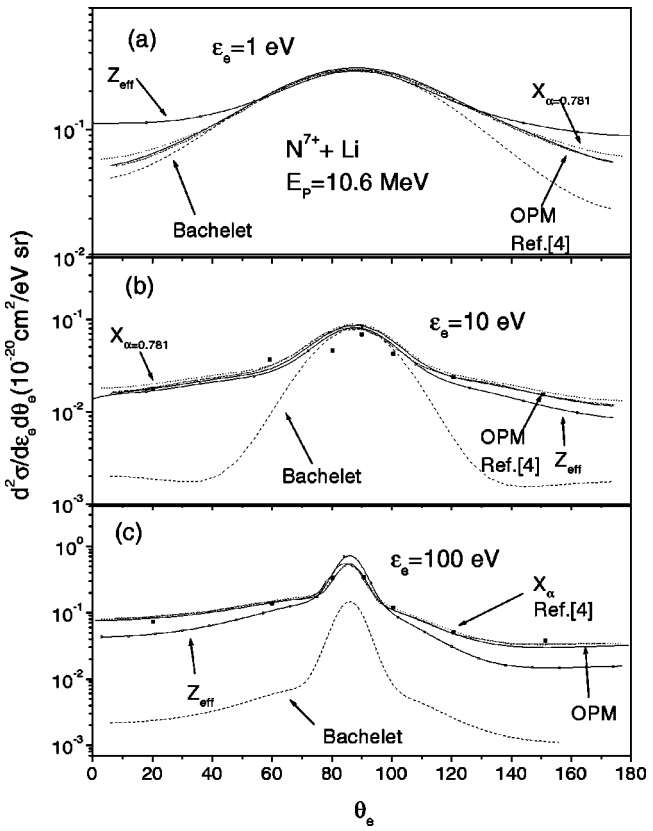

FIG. 4. DDCS for 10.6 MeV N^{+7} on Li as a function of the ejected electron angle θ_e for some ejected electron energy ϵ_e. Solid line, OPM potential; dashed line, Bachelet's pseudopontential; dotted line, $X\alpha$ ($\alpha = 0.781$); the short-dash-dotted line, $Z_{\text{eff}} = 2.2261$ and 1.2532; dash-dot-dotted lines, theoretical calculation of Ref. [4]; and the square, experimental results of the same group. In (a) $\epsilon_e = 1$ eV, (b) $\epsilon_e = 10$ eV, and in (c) $\epsilon_e = 100$ eV.

Figures 7(a)–(d) present the TCS for ionization of lithium atoms, as a function of the projectile impact energy, Figs. 7(a)–(b) refer to collisions with H^+, Figs. 7(c)–(d) collisions with He^{2+}. Together with our results, we show the experimental results of Shah *et al.* [2].

B. Discussion

At very low electron ejection energies, the electron emission is expected to be dominated by dipole transitions produced mainly in large impact parameter collisions. The Bethe or dipole approximation [7,36] shows that this approach is good when the product that appears in Eqs. (2.7) and (2.8) is smaller than one, that is,

$$qr < 1. \tag{3.1}$$

This condition is fulfilled when the initial electronic density is localized close to the nucleus (like a $1s$ orbital of lithium) or $v_p \gg v_a$, where v_a is the active bound electron velocity; the momentum transfer in a soft collision is small ($q_{\min} \simeq (k_e^2/2 + |\varepsilon_i|)/v_p$). In the second case, the interaction of the

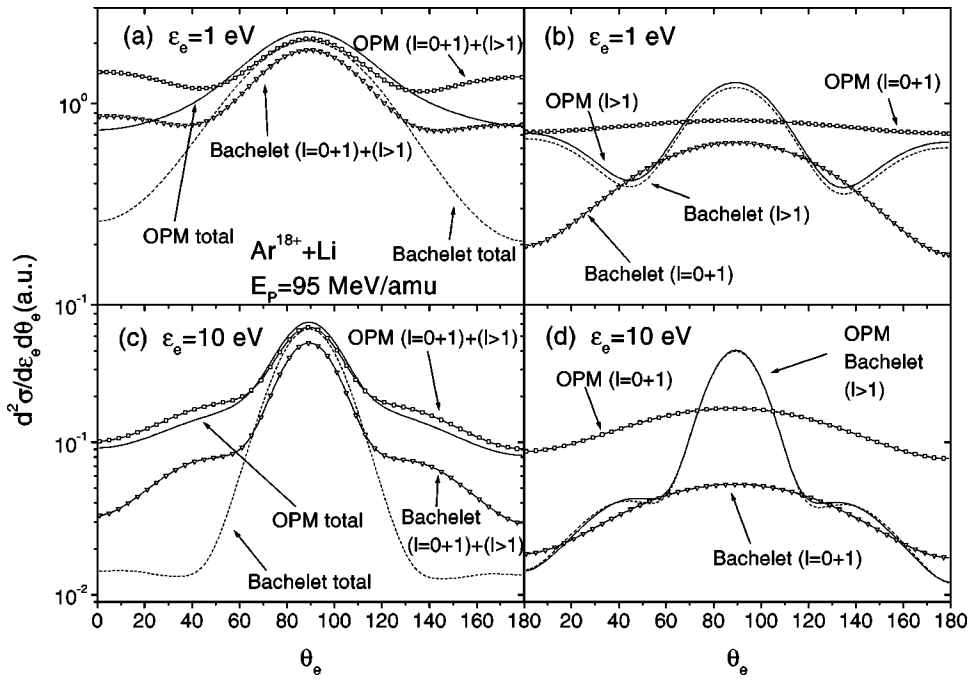

FIG. 5. DDCS and multipole contributions (a.u.) for 95-MeV Ar^{+18} on Li for the $2s$ ionization. (a) $\epsilon_e=1$ eV. Solid line, total contribuion for OPM potential; dashed line, total contribuion for Bachelet's pseudopotential; line plus square, without interference between the $l=0,1$ terms and the remaining terms for OPM potential; line plus triangle, whithout interference between the $l=0,1$ terms and the reminding terms for Bachelet's pseudopotential; (b) $\epsilon_e=1$ eV. Solid line, contribution from $l>1$ for OPM potential, dashed line, contribution from $l>1$ Bachelet's pseudopotential; line plus square, dipole plus monopole contribution for OPM potential; line plus triangles, dipole plus monopole contribution for Bachelet's pseudopotential; (c) same of (a) for $\epsilon_e=10$ eV; (d) same of (b) for $\epsilon_e=10$ eV.

projectile with the target may be treated as an interaction with a photon [5]. The angular distribution associated with those soft electrons are usually broad and should be symmetric around 90°.

On the other hand, higher electron energies with larger momentum transfer are characterized by a maximum corresponding to the binary encounter (BE) peak, which moves to forward angles at higher energies. By the BE theory, the energy position of this maximum is related to the kinetic energy and mass of the projectile T/m_p and to the ionization energy ε_l by

$$\varepsilon_{BE}=\frac{4T}{M_P}\cos\theta_e-\varepsilon_l. \tag{3.2}$$

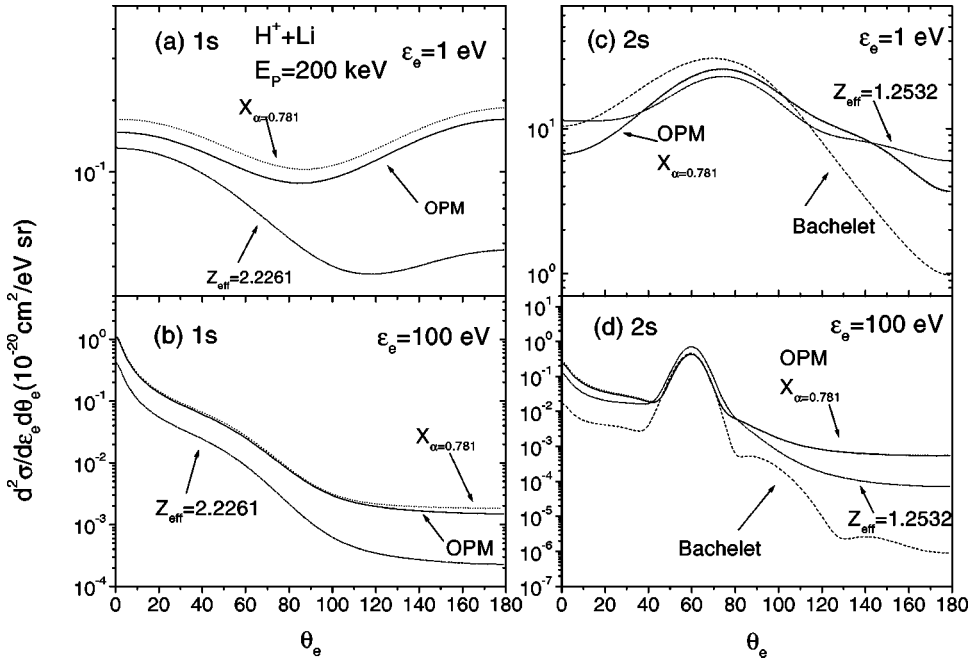

FIG. 6. DDCS for 200-keV protons on Li as a function of θ_e for some ejected electron energy. Solid line, OPM potential; dashed line, Bachelet's pseudopontential; dotted line, $X\alpha$ ($\alpha=0.781$); short-dash-dotted line, Coulomb potentials. Ionization of the $1s$ electron ($Z_{\rm eff}=2.2261$) for (a) $\epsilon_e=1$ eV and (b) $\epsilon_e=100$ eV. Ionization of the $2s$ electron ($Z_{\rm eff}=1.2532$) for (c) $\epsilon_e=1$ eV and (d) $\epsilon_e=100$ eV.

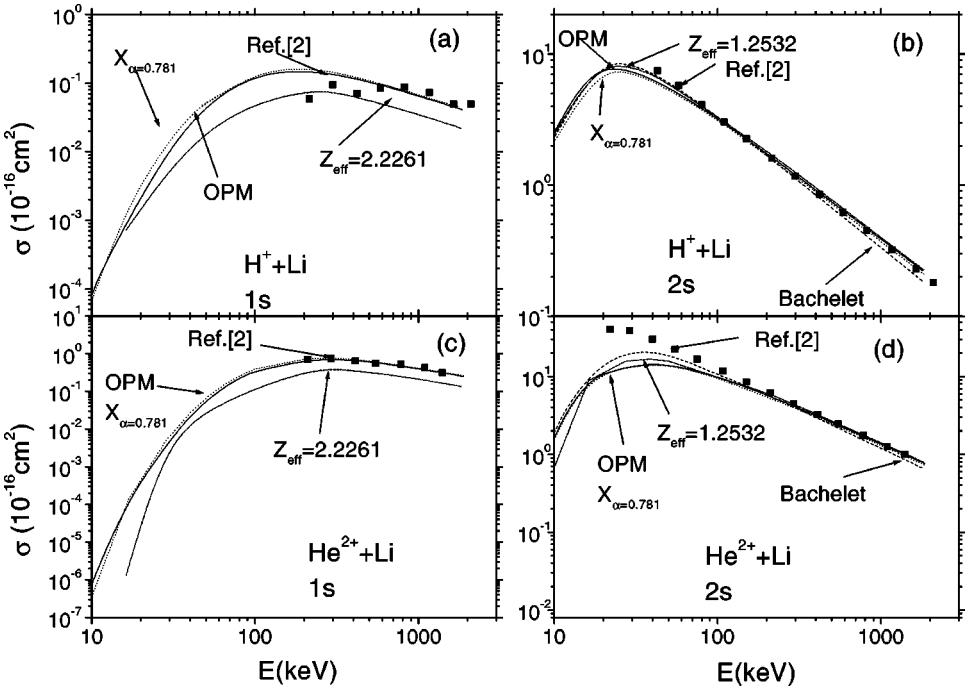

FIG. 7. TCS for 200 keV H^+ (a) and (b) and He^{2+} (c) and (d) on Li as a function of the projectile energy E_p (in eV). Square, experimental results of Ref. [2]; solid line, OPM potential; dashed line, Bachelet's pseudopontential; dotted line, $X\alpha$ ($=0.781$) potential; short-dash-dotted line, Coulomb potentials. Ionization of the $1s$ electron ($Z_{\text{eff}}=2.2261$) for (a) and (c). Ionization of the $2s$ electron ($Z_{\text{eff}}=1.2532$) for (b) and (d).

The shape of the peak is described by a Compton profile, which is related to the Fourier transform of the initial wave function. Obviously, for high-electron energy, large angular momenta components are necessary to describe the DDCS.

In the following, the arguments delineated above will be used in order to discuss the Figs. 4 to 6 already presented.

Figure 4 show that our present $X\alpha$ ($\alpha=0.781$) potential results agree with those of Skogvall *et al.* [which is a $X\alpha(\alpha=2/3)$] and no significant difference is observed between them and our OPM potential, except for the peak maximum value, corresponding to high energies at $\theta=90°$. This is not surprising since, as shown in Sec. II B, the numerical results coming from different potentials are very similar for the discrete and continuum electron wave functions. On the other hand, the results obtained with the Z_{eff} continuum state present significant difference for the lower and higher electron energies, being greater for the orbital $1s$. The differences are more pronounced for backscattering, these electrons being more influenced by the target potential since much of the backscattering electrons are produced in process of double collisions [37].

For low electron energies, where the $1s$ contribution is not so important, the Bachelet's calculations reproduce well the results of the OPM model potential and those of Skogvall *et al.* for $\varepsilon_e=1$ and 10 eV very close to 90°, i.e., the BE peak. For all other angles, the Bachelet's potential described very poorly the results for 1 eV and 10 eV. This can be understood looking for two aspects. First, different from the other $2s$ bounded wave functions, the one calculated by the Bachelet's potential does not have nodes, so there is no separation between the inner and outer part of this orbital as will be discussed below. Second, the backscattered electrons with smaller kinetic energies are more affected by the target electrons represented by the potentials. Another significant signature of this effect is related to the behavior of the internal phase shifts as a function of l for the different potentials, as shown in Fig. 3. As shown there, δ_l^{in} is greater for low values of l.

As mentioned before, the $1s$ orbital contribution comes mainly from $l=0$ and 1 for low ejected energy, but its contribution grows with ϵ_e. This can explain the smaller value of the BE profile for 100 eV of Fig. 4(c) for the Bachelet's calculations where no $1s$ orbital is available. It is interesting to note that in Figs. 4(a) and 4(b), although the angular distribution of the slower electrons are flatter than those of higher energies presented in Fig. 4(c), a pronounced BE peak corresponding to the $2s$ electron is observed. Skogvall *et al.* [4] analyzed their results in terms of multipoles for the $1s$ and $2s$ 1-eV electron ejection energy. They found that for the $1s$ orbital the dipole transitions dominate the electron production for all angles. For the $2s$ orbital, they observed that only 25% of the maximum can be explained by dipole transitions. They then concluded that for the $2s$ initial state, 75% of the 1 eV electrons are produced by BE. For higher electron energies, they also attributed the sharp peak to the $2s$ orbital as the Compton profile for this orbital is narrower than the one of the $1s$ orbital. In fact, the BE for the latter orbital is spread out over the entire angular range.

It is worth mentioning that, even for the total ionization cross section, Peach [9] has already observed that the $2s$ ionization cannot be treated as a dipole transition. The author found that the major contribution comes not from optically allowed transitions ($l=1$) as in the case of H and He targets, but from $l=2$ and 3.

Stolterfoht *et al.* [5] used, in order to explain their experimental data of ionization of soft electrons, a plane-wave Born approximation with a peaking approximation [38] and *Hartree-Fock-Slater* $X\alpha$ [14] initial wave functions. They related this approximation to a BE, related to two-body effects associated with angular momenta $l>1$, and the difference between the approximation and the experimental data

fitted with $A+B\sin^2\theta+C\cos\theta$ (monopole plus dipole terms), was attributed to a three-body process.

This interpretation is not completely satisfactory for the DDCS of the $2s$ ionization. In Fig. 5 we can see that the contribution of the interference terms between $l=0,1$ and the other multipoles are not negligible for electrons emitted with an energy of 10 eV and are of great importance to explain the shape of the 1-eV DDCS. The importance of the interference terms was observed before by Voitkiv *et al.* [36] within the FBA for the hydrogen ionization at high energies, where they show the importance of the dipole-quadrupole interference term in the DDCS.

Although the $1s$ ionization is basically a dipolar one, this does not happen with electrons emitted from a $2s$ shell as we can see in Fig. 5. The $l>1$ contribution is the most important in the binary encounter region and the dipole plus monopole contributions are important in the small and large angles, as can be verified in Figs. 5(b) and 5(d). But we can see in Figs. 5(a) and 5(c) that the interference terms between the monopole plus dipole and the others are important for an 1 eV electron and are not negligible for an electron energy of 10 eV. In this last case, the influence of the interference terms are more important for small and large angles, that is, when the relative contribution of $l>1$ diminishes.

A multipole decomposition, as done in Fig. 5, allows us to compare the influence of the potentials in the DDCS. For example, in the Bachelet's potential, the components $l=0$ and $l=1$ of the continuum wave functions are the most affected by the unphysically repulsive internal potential. For the energies considered here, the other Components are basically coulombic and consequently, the OPM's and Bachelet's $l>1$ contributions are almost equal.

Figure 6 show that for 200-keV H^+ collision, the binding energy plays an important role in the process especially for ionization from an $1s$ orbital since the value of $q_{\min}$ ($q_{\min}\simeq(k_e^2/2+|\varepsilon_i|)/v_p$) depends critically of this energy. This is due to the relatively low velocity of the projectile. In particular, the position of the binary peak is modified with respect to the other cases. A multipole expansion like $A+B\cos^2\theta+C\cos\theta$ describes the $1s$ angular distributions for 1 eV [Fig. 6(a)] showing evidence of contributions from $l=0,1$ (with $m=0$). The crossed term is almost zero for the OPM and $X\alpha$ ($\alpha=0.781$) wave functions but important for the Z_{eff} one. In the backscattering region, the large charge of the Z_{eff} continuum wave function is responsible for its low intensity relative to the other ones. A difference up to 20% is observed in the $1s$ DDCS between OPM and Xα ($\alpha=0.781$), this difference comes from the two slightly different orbital energies calculated for the $1s$ orbital, respectively, 2.0799 and 1.948 u.a.

For the $2s$ shell, Figs. 6(c) 6(d) show that the results with the Bachelet's pseudopotential agree with the others for the BE region but presents wrong intensities and also some spurious oscillations at angles larger than 90°. We have verified that, in this case, large angular momentum values are necessary to converge this result. At the BE region the DDCS is basically dominated by the small transfer momentum q values of the Fourier transform of the initial state [38], reflecting the region of large r in the real space, where the Bachelet's potential gives a proper description. For the large ejected electrons angles and 200-keV impact energy, the contribution of large transfer momentum q becomes important, showing evidence of an eventual incorrect trend of the internal part of the bound wave function. This fact is responsible for the appearance of spurious oscillations in the nonbinary region of the DDCS calculated from Bachelet's potential as shown in Fig. 6(c) and 6(d).

In the limit of large distances, the ionized electron feels a net charge of -1, not described by the Z_{eff} model, and this is reflected in the DDCS calculated using the Z_{eff}, as can be seen in Fig. 6. For a deeper discussion, see for instance Ref. [38].

One evidence of the postcollisional interaction can be appreciated in Figs. 6(b) and 6(d) for the small-angle scattering. In this case, the relative slow velocity between the electron and the projectile favors the electron capture to continuum.

One surprising characteristic of the Figs. 7(b) and 7(d), which correspond to the $2s$ ionization, is the good agreement between the TCS calculated with the distinct potentials. Even our poorest descriptions, that is, the Z_{eff} and Bachelet potentials, that do not appropriately describe the DDCS, agree with those calculated with the more precise OPM and X_α ones. Nevertheless, the Bachelet's cross section decreases more quickly than the others, probably due to the importance of the internal part of the initial wave function in the high-energy regime. Our calculations agree well with the experimental results of Ref. [2] for energies greater than 100 keV, where the CDW-EIS approximation is valid.

In the ionization from an $1s$ orbital [Figs. 7(a) and 7(c)], we do not have Bachelet's total cross section. As the $1s$ ionization is not directly measured, the experimental data shown here represent an estimate of this value.

IV. CONCLUSIONS

We have analyzed the dependence of the DDCS and the TCS upon the description of the atomic discrete and continuum electronic wave function, comparing these cross sections with the available theoretical and experimental results. We point out that, for the $2s$ ionization, the TCS results are shown to be much less sensible to the description of the target by wave functions obtained employing different potentials than for the $1s$ case, where the Z_{eff} presents remarkable differences from the other ones.

As the wave functions generated by the OPM and $X\alpha$ ($\alpha=0.781$) potentials are quite similar (see Figs. 2 and 3), it follows that their DDCS and TCS are nearly equivalent. This is a manifestation of the small exchange effect for the lithium atom contrary to the results obtained for larger atoms [16]. The pseudopotential of Bachelet *et al.* presents a wrong behavior for small values of r, as Fig. 1 shows. As a consequence, the DDCS with the wave functions generated by this potential, fail to reproduce the correct angular dependence, except for the BE peak. It seems that, although this kind of pseudopotential may be successfully used in other branches of physics and chemistry, it presents serious problems for

ion-atom collisions especially when the inner part of the potential is probed, i.e., for small impact parameter. It is expected that other pseudopotentials like the ones discussed by G. Peach [39] would give similar results.

The present results confirm the study of Skogvall *et al.* [5], namely, the $1s$ ionization is basically dominated by dipolar terms, but also point to a different situation for the $2s$ ionization. In this last case, the BE region is dominated by the $l \geqslant 2$ terms and the interference terms between monopole dipole and those terms is negligible. Outside this region, i.e., for small and for large scattering angles, these interference terms cannot be neglected.

ACKNOWLEDGMENTS

The authors would like to thank N. V. de Castro Faria and L. F. S. Coelho for carefully reading the manuscript. This work was partially supported by the Brazilian Agencies CNPq, FUJB, and FAPERJ.

[1] J. Schweinzer, E. Wolfrum, F. Aumayr, M. Pöckl, H.P. Winter, R.P. Schorm, E. Hintz, and A. Unterreiter, Plasma Phys. Controlled Fusion **34**, 1173 (1992); R.P. Schorn, E. Wolfrum, F. Aumayr, E. Hintz, D. Rusbuldt, and H. Winter, Nucl. Fusion **32**, 351 (1992).
[2] M.B. Shah, D.S. Elliott, and H.B. Gilbody, J. Phys. B **18**, 4245 (1985).
[3] R.D. DuBois, Phys. Rev. A **32**, 3319 (1985).
[4] B. Skogvall, M. Tschersich, J. Tanis, B. Sulik, L. Gulyás, M. Grether, and N. Stolterfoht, Nucl. Instrum. Methods Phys. Res. B **124**, 186 (1997).
[5] N. Stolterfoht, J.Y. Chesnel, M. Grether, J.A. Tanis, B. Skogvall, F. Frémont, D. Lecler, D. Hennecart, X. Husson, J.P. Grandin, C. Koncz, L. Gulyás, and B. Sulik, Phys. Rev. A **59**, 1262 (1999); N. Stolterfoht, J.Y. Chesnel, M. Grether, B. Skogvall, F. Frémont, D. Lecler, D. Hennecart, X. Husson, J.P. Grandin, B. Sulik, L. Gulyás, and J.A. Tanis, Phys. Rev. Lett. **80**, 4649 (1998).
[6] D. Wutte, R.K. Janev, F. Aumayr, M. Schneider, J. Schweinzer, J.J. Smith, and HP. Winter, At. Data Nucl. Data Tables **65**, 155 (1997).
[7] M.R.C. McDowell and J.P. Coleman, in *Introduction to the Theory of Ion-Atom Collisions* (North-Holland, Amsterdam, 1970).
[8] M.R.C. McDowell and G. Peach, Phys. Rev. **121**, 1383 (1961).
[9] G. Peach, Proc. Phys. Soc. London **85**, 709 (1965).
[10] D.S.F. Crothers and J.F. McCann, J. Phys. B **16**, 3229 (1983).
[11] M. McCartney and D.S.F. Crothers, J. Phys. B **26**, 4561 (1993).
[12] E.C. Clementi and C. Roetti, At. Data Nucl. Data Tables **14**, 177 (1974).
[13] M.D. Sánchez, W. Cravero, and C.R. Garibotti, Nucl. Instrum. Methods Phys. Res. B **142**, 281 (1998).
[14] J.C. Slater, Phys. Rev. **81**, 385 (1951).
[15] F. Herman and S. Skillman, *Atomic Structure Calculations* (Prentice-Hall, Englewood Cliffs, NJ, 1963).
[16] T. Kirchner, L. Gulyás, H.J. Lüdde, E. Engel, and R.M. Dreizler, Phys. Rev. A **58**, 2063 (1998); T. Kirchner, L. Gulyás, H.J. Lüdde, A. Henne, E. Engel, and R.M. Dreizler, Phys. Rev. Lett. **79**, 1658 (1997).
[17] H.J. Lüdde, A. Henne, T. Kirchner, and R.M. Dreizler, J. Phys. B **29**, 4423 (1996).
[18] G.B. Bachelet, D.R. Hamann, and M. Schlüter, Phys. Rev. B **26**, 4199 (1982).
[19] J.D. Talman, Comput. Phys. Commun. **54**, 85 (1989).
[20] D. A. Varshalovich, A. N. Moskalev, and V. K. Khersonskii, *Quantum Theory of Angular Momentum* (World Scientific, Singapore, 1988).
[21] S.T. Manson, L.H. Toburen, D.H. Madison, and N. Stolterfoht, Phys. Rev. A **12**, 60 (1975).
[22] T. N. Chang, *Many-Body Theory of Atomic Structure and Photoionization* (World Scientific, Singapore, 1993).
[23] M. Venuti, A. Lisini, and P. Decleva, J. Phys. B **29**, 5315 (1996).
[24] L.E. Machado, M.T. Lee, and L.M. Brescansin, J. Chem. Phys. **110**, 7228 (1999); A.L. Monzani, L.E. Machado, M.T. Lee, and A.M. Machado, Phys. Rev. A **60**, R21 (1999).
[25] B. Ritchie, M.S. Pindzola, and W.R. Garrett, Phys. Rev. A **23**, 2905 (1981).
[26] W. Kohn and L.J. Sham, Phys. Rev. A **140**, 1133 (1965).
[27] L. Gulyás, P.D. Fainstein, and A. Salin, J. Phys. B **28**, 245 (1995).
[28] Karlheinz Schwarz, Phys. Rev. B **5**, 2466 (1972).
[29] M.D. Pauli, http://www.uwm.edu/ mpauli/
[30] R.T. Sharp and G.K. Horton, Phys. Rev. **30**, 317 (1955).
[31] J.D. Talman and W.F. Shadwick, Phys. Rev. A **14**, 36 (1976).
[32] L. Szasz, *The Electronic Structure of Atoms* (Wiley, New York, 1992).
[33] F. Salvat, J.M. Fernández-Varea, and W. Williamson, Jr., Comput. Phys. Commun. **90**, 151 (1995).
[34] D.S. Crothers and M. McCartney, Comput. Phys. Commun. **72**, 288 (1992).
[35] D. Marshall, M. McCartney, and D.S.F. Crothers, Comput. Phys. Commun. **86**, 279 (1995).
[36] A.B. Voitkiv, N. Grun, and W. Scheid, J. Phys. B **32**, 4741 (1999).
[37] G. Gasaneo, W. Cravero, M.D. Sanchez, and C.R. Garibotti, Phys. Rev. A **54**, 439 (1996).
[38] N. Stolterfoht, R. D. DuBois, and R. D. Rivarola, *Electron Emission in Heavy Ion-Atom Collisions* (Springer-Verlag, Berlin, 1997).
[39] G. Peach, Comments At. Mol. Phys. **11**, 101 (1982).